Remmelzwaal, S., Dixon, S., Parkinson, I., Schmidt, D., Monteiro, F., Sexton, P. F., Fehr, M. A., Peacock, C., Donnadieu, Y., & James, R. (2019). Investigating Ocean Deoxygenation During the PETM Through the Cr Isotopic Signature of Foraminifera. *Paleoceanography and Paleoclimatology*, *34*(6), 917-929. https://doi.org/10.1029/2018PA003372

Manuscript for submission to Paleoceanography and Paleoclimatology

Investigating ocean deoxygenation during the PETM through the Cr isotopic signature of foraminifera

Serginio R. C. Remmelzwaal[1]*, Sophie Dixon[2], Ian J. Parkinson[1], Daniela N. Schmidt[1], Fanny M. Monteiro[3], Philip Sexton[2], Manuela A. Fehr[2.4], Caroline Peacock[5], Yannick Donnadieu[6.7], Rachael H. James[8]

[1]School of Earth Sciences, University of Bristol, Wills Memorial Building, Queens Road, Bristol, BS8 1RJ, UK

[2]School of Environment, Earth and Ecosystem Sciences, The Open University, Walton Hall, Milton Keynes, MK7 6AA, UK

[3]School of Geographical Sciences, University of Bristol, University Road, Bristol, BS8 1SS, UK

[4]Institut für Geochemie und Petrologie, ETH Zürich, Clausiusstr. 25, CH-8092 Zürich, Switzerland

[5]School of Earth and Environment, University of Leeds, Maths/Earth and Environment Building, Leeds, LS2 9JT, UK

[6]Laboratoire des Sciences du Climat et de l'Environnement, UMR CNRS-CEA Saclay, Orme des Merisiers, 91 190 Saint-Aubin, France

[7]Aix-Marseille Université, CNRS, IRD, CEREGE, 13545 Aix-en-Provence, France

[8]Ocean and Earth Science, National Oceanography Centre Southampton, University of Southampton, European Way, Southampton SO14 3ZH, UK

***Corresponding author: serginio.remmelzwaal@bristol.ac.uk**

Key Points:

- Chromium isotope variations in foraminifera are controlled by the local redox state.
- Deoxygenation during the Palaeocene-Eocene Thermal Maximum caused widespread hypoxia throughout the global oceans.
- Ocean water warming cannot fully account for the reported extent of open ocean deoxygenation during the Paleocene Eocene Thermal Maximum.

Abstract

Over the past several decades, oxygen minimum zones have rapidly expanded due to rising temperatures raising concerns about the impacts of future climate change. One way to better understand the drivers behind this expansion is to evaluate the links between climate and seawater deoxygenation in the past especially in times of geologically abrupt climate change such as the Palaeocene-Eocene Thermal Maximum (PETM), a well characterised period of rapid warming ~56 million years ago. We have developed and applied the novel redox proxies of foraminiferal Cr isotopes ($\delta^{53}Cr$) and Ce anomalies (Ce/Ce*) to assess changes in paleo-redox conditions arising from changes in oxygen availability. Both $\delta^{53}Cr$ and Cr concentrations decrease notably over the PETM at intermediate to upper abyssal water depths, indicative of widespread reductions in dissolved oxygen concentrations. An apparent correlation between the sizes of $\delta^{53}Cr$ and benthic $\delta^{18}O$ excursions during the PETM suggests temperature is one of the main controlling factors of deoxygenation in the open ocean. ODP Sites 1210 in the Pacific and 1263 in the Southeast Atlantic suggest that deoxygenation is associated with warming and circulation changes, as supported by Ce/Ce* data. Our geochemical data are supported by simulations from an intermediate complexity climate model (cGENIE), which show that during the PETM anoxia was mostly restricted to the Tethys Sea, while hypoxia was more widespread as a result of increasing atmospheric CO_2 (from 1 to 6 times pre-industrial values).

Keywords: Chromium, Cerium, Deoxygenation, Foraminifera, Hypoxia, PETM

1. Introduction

As emitted greenhouse gasses accumulate in the atmosphere, temperatures are rising in both the atmosphere and the oceans with unclear consequences for marine ecosystems (Pörtner et al., 2014). One of the hazards associated with global warming is a decrease in oceanic dissolved oxygen content. Over the past 50 years O_2 levels have been steadily declining, leading to the expansion of so-called oxygen minimum zones – areas of hypoxic to suboxic levels of O_2 at intermediate water depths due to the decreased solubility of O_2 and increased metabolic rates of heterotrophic microbes as temperatures rise (Keeling et al., 2010). Understanding the effect of ocean warming on the expansion and intensification of oxygen minimum zones and deep ocean hypoxia is particularly needed (Pörtner et al., 2014). In this study, we assess the development of ocean hypoxia under high temperatures by using extreme warming in the geological past as an analogue for modern anthropogenic warming.

The climate of the Palaeocene and Eocene greenhouse periods experienced several extreme transient warming events of which the largest, the Palaeocene-Eocene Thermal Maximum (PETM; e.g. Cramer et al., 2003) occurred about 56 Ma (Westerhold et al., 2009). The PETM is a particularly pertinent time interval because of its parallels to present-day anthropogenic global warming (Pörtner et al., 2014). Global climate warmed rapidly by ~ 5 degrees Celsius (Dunkley-Jones et al., 2013) within 4,000 – 20,000 years (Zeebe et al., 2016; Gutjahr et al., 2017), with warming lasting for ~200 kyr (Röhl et al., 2007). The cause of the carbon isotope excursion (CIE) towards lighter $\delta^{13}C$ is still heavily debated (Gutjahr et al., 2017) with much of the literature pointing toward an injection of biogenic methane into the ocean-atmosphere system (e.g. Svensen et al., 2004). The injection of large amounts of carbon resulted in a decrease in alkalinity and intense dissolution of $CaCO_3$ (Penman et al., 2016). The estimated change in pH was about -0.3 units in the surface ocean (Penman et al., 2014; Gutjahr et al., 2017) with an accompanying rise in the calcite compensation depth (CCD) of up to 2 km in the Atlantic Ocean (Zachos et al., 2005; Penman et al., 2016) though significantly less in the Pacific (>500 m; Colosimo et al., 2006).

The warming of the ocean, increased nutrient run-off, enhanced stratification, and the oxidation of a large body of reduced carbon are all suggested to have reduced oxygen levels in the oceans during the PETM (Nicolo et al., 2010; Dickson et al., 2012; Pälike et al., 2014; Chang et al., 2018). Deoxygenated bottom waters are thought to have been commonplace in marginal settings (e.g. Dickson et al., 2014) and oxygen minimum zones have been suggested to have expanded (Chun et al., 2010; Pälike et al., 2014; Zhou et al., 2016). The presence of geochemical indicators for deoxygenation in the Atlantic, an absence of these in the Pacific Ocean, and the difference in change in the CCD strongly suggest the carbon source was situated in the Atlantic Ocean (Chun et al., 2010; Pälike et al., 2014; Zhou et al., 2016). We propose here to further investigate the presence and development of hypoxia during the PETM in the Atlantic and Pacific using Cr isotopes in foraminifera.

Chromium isotopes have received attention in the past few years owing to their potential for reconstructing the paleoredox state of the oceans (e.g. Bonnand et al., 2013; Reinhard et al., 2014). Chromium has multiple valence states and is therefore redox sensitive. In the marine environment, Cr can occur as either Cr(III) or Cr(VI) species, with Cr(VI)-oxyanions the dominant species in oxic seawater (Cranston and Murray, 1978). Chromium has four stable isotopes of which the difference in the $^{53}Cr/^{52}Cr$ ratio compared to NIST SRM979 is reported in the delta notation as $\delta^{53}Cr_{SRM979}$, where $\delta^{53}Cr_{SRM979} = 1000*[(^{53}Cr/^{52}Cr)_{sample} - (^{53}Cr/^{52}Cr)_{SRM979}] / (^{53}Cr/^{52}Cr)_{SRM979}$. As seawater becomes less oxic, Cr(VI) will be reduced to Cr(III) which is removed into oceanic sediments, resulting in lower dissolved Cr concentrations. The reduction of Cr is accompanied by a substantial isotope fractionation of up to 7‰ (Ellis et al., 2002). Recent studies have shown that the $\delta^{53}Cr$ of modern seawater is heterogeneous varying between 0.1 – 1.8 ‰, which can partly be explained by a short residence time of ~3,000 years (Qin & Wang, 2017; Goring-Harford et al., 2018) relative to the average ocean overturning time of ~1500 years. There appears to be a negative correlation between [Cr] and $\delta^{53}Cr$ in seawater samples measured to date (Scheiderich et al., 2015; Paulukat et al., 2016) that has been attributed to partial reduction of Cr(VI) in surface waters and oxygen minimum zones (with a $\Delta_{Cr(III)-}$

$_{Cr(VI)}$ of -0.79‰), coupled with Cr(III) re-oxidation in deep waters (Scheiderich et al., 2015; Paulukat et al., 2016).

Experimental data and studies on carbonates show that Cr is incorporated into the calcite lattice of carbonates (Tang et al., 2007; Bonnand et al., 2013) as a chromate ion and therefore marine carbonate records can be used as a potential archive for seawater Cr. A recent investigation into seawater controls on the Cr isotopic composition of core-top foraminifera (Wang et al., 2017) left open questions as to what might drive incorporation of Cr into foraminifera. No direct calibrations of this proxy in foraminiferal calcite have been performed. However, recent work has shown that while some Cr is incorporated during calcification most Cr in sedimentary foraminifera has a post-depositional origin and therefore will record bottom and pore water Cr compositions (Remmelzwaal et al., in review). Remmelzwaal et al. (in review) also demonstrated that foraminiferal $\delta^{53}Cr$ values are not species dependent, but rather dependent on foraminiferal test size meaning that the surface area/volume ratio controls Cr exchange between the test and bottom water and/or sediment pore waters. Questions around the empirical relationship between $\delta^{53}Cr$ and $[O_2]$ as well as potential dissolution effects remain unanswered. We thus interpret $\delta^{53}Cr$ data here in a qualitative sense, in terms of the sign of change, as an indicator of bottom and pore water ocean deoxygenation.

To better constrain bottom water ocean deoxygenation during the PETM, we combine Cr isotope data with measurements of cerium (Ce), a potentially useful rare earth element (REE) to reconstruct oxidation states (e.g. Zhou et al., 2016). Unlike most REEs, Ce has two oxidation states, Ce(III) and Ce(IV), and like Cr is redox sensitive. Modern seawater has a characteristic negative Ce anomaly. This anomaly has been suggested to have been caused by the oxidation of Ce(III) to the insoluble and particle-reactive Ce(IV) in surface waters and estuaries where seawater is consequently depleted in Ce with respect to La, Pr and Nd (De Baar et al., 1988). In anoxic waters Ce concentrations are high and the Ce anomaly vanishes or even becomes slightly positive (De Baar et al., 1988). Ce/Ce* values (defined in Section 2.3.2) are approximately 1.0 in anoxic seawater, 0.5-1.0 in hypoxic pore waters

and lower than 0.5 for oxic seawater (Zhou et al., 2016). Foraminiferal cerium mostly resides in authigenic ferromanganese coatings that form after sediment deposition (Palmer et al., 1985).

In this study, we investigate the development of open ocean deoxygenation during the PETM using the foraminiferal redox proxies δ^{53}Cr and Ce/Ce*. We compare our data with published geochemical, sedimentological and micropalaeontological studies that inform on redox conditions during the PETM. We also perform some ocean biogeochemical model simulations; this model-data comparison allows us to assess the evolution of ocean deoxygenation in intermediate and upper abyssal waters, and the extent to which the oceans experienced hypoxia and anoxia.

2. Material and Methods

2.1 Sample site selection

Our geochemical data are derived from three sites drilled by the Deep-Sea Drilling Program (DSDP) and Ocean Drilling Program (ODP): DSDP Site 401 is located in the Bay of Biscay (north-eastern Atlantic) with a paleodepth of 1900 m, ODP Site 1263 is on Walvis Ridge (south-eastern Atlantic) with a palaeodepth of 1500 m, and ODP Site 1210 is on Shatsky Rise (North Pacific) with a palaeodepth of 2400 m (Figure 1; Pälike et al., 2014, and references therein). Site 1210 is located in the North Pacific where more vigorous deep-water formation has been suggested to have occurred during the PETM (Tripati & Elderfield, 2005; Lunt et al., 2010), whereas a slowdown purportedly occurred in the South Atlantic (Site 1263) (Tripati & Elderfield, 2005). It must be noted, however, that there is no consensus on the site of deep-water formation during the PETM with the North Atlantic as location of downwelling (Bice & Marotzke, 2002; Nunes & Norris, 2006; Alexander et al., 2015). Site 1263 was located near a major oxygen minimum zone (Chun et al., 2010). Site 401 was in the comparatively narrow North Atlantic that was gradually widening in association with major volcanic activity during the Palaeocene-Eocene (Svensen et al., 2004).

2.2 Age models

Age models were derived from the cyclostratigraphic analyses by Gutjahr et al. (2017) for Site 401, Westerhold et al. (2008) for Site 1210, and Röhl et al. (2007) for Site 1263. These were anchored to a timescale following the age constraint of the PETM by Westerhold et al. (2009). Linear sedimentation rates were used to calculate the ages for all the data plotted.

2.3 Analytical methods

2.3.1 Sample processing

Sediment samples (n = 87) of 10-20 cm^3 were wet sieved with a 63 µm sieve. Coarse fractions are the dry mass of the particles larger than 63 µm as the weight percentage of the dry mass of the total sample prior to sieving. A mixture of planktic foraminiferal species (*Morozovella* spp., *Acarinina* spp. and *Subbotina* spp.) was picked from these samples to obtain approximately 1,000 specimens (or about 0.11 g). At Sites 1210 and 1263, foraminifera are moderately well-preserved before the PETM, but preservation rapidly deteriorates during the onset of the CIE and improves again during the CIE recovery (Kelly et al., 2005; Petrizzo, 2007). At Site 401, foraminifera are generally well-preserved throughout the studied interval (Pardo et al., 1997). Samples were cleaned by gently cracking open the foraminiferal tests, with subsequent removal of clay particles and organic matter by ultrasonication in Milli-Q (MQ) grade water and by leaching in alkali buffered H_2O_2, respectively (Barker et al., 2003). Analysis of the chemical composition of marine Fe-Mn-rich crusts show that these have relatively low Cr concentrations (16 - 47 ppm Cr; Hein & Koschinsky, 2014) and therefore the Fe-Mn coatings were not removed to preserve as much of the calcite as possible for analysis (Remmelzwaal et al., in review).

2.3.2 Trace element analysis

Cleaned samples of ~0.01 g were dissolved in cold 0.5M acetic acid, dried down to incipient dryness and subsequently were dissolved and diluted with 2% HNO_3 acid by ~4000 times to produce a 100 ppm Ca solution. A suite of synthetic standards containing 40 trace elements at a variety of concentrations and doped with 100 ppm Ca were used to produce a calibration curve. Rare earth elements and Cr concentrations were measured in He and O_2 collision mode respectively on an Agilent 7500s ICP-QQQ-MS (Triple Quadrupole ICP-MS) at the Open University. Rare earth element concentrations are normalised to Post Archaean Australian Shale (PAAS) concentrations (Taylor & McLennan, 1985). Anomalies in Ce are expressed as $Ce/Ce^* = (Ce/Ce_{PAAS})/[Pr/Pr_{PAAS}*(Pr/Pr_{PAAS})/(Nd/Nd_{PAAS})]$ (Tostevin et al., 2016). Measurements are reproducible within ~ ±2% for Cr and ~ ±9% for Ce/Ce* based on replicate analysis of the carbonate standard reference material JDo-1.

2.3.3 Chromium isotope analysis

Approximately 0.1 g of sample (down to 0.03 g during the height of the dissolution event at ODP Site 1263) was dissolved by ultrasonication in 0.5M acetic acid to prevent any potential leaching of any remaining detrital material left after cleaning. Chromium was subsequently extracted following the cation exchange chromatographic separation procedures described in Bonnand et al. (2011) with procedural blank Cr contributions of ~0.2 ng. JDo-1 was subjected to the same chemistry protocol as the samples. Chromium isotopes were measured on a ThermoFisher Scientific Neptune MC-ICP-MS at the University of Bristol by using a ^{50}Cr-^{54}Cr double-spike technique following Bonnand et al. (2011). The average value obtained for JDo-1 is $\delta^{53}Cr = 1.715 \pm 0.059$ (2σ, $n = 8$), which is within error of previously published values of $\delta^{53}Cr = 1.719 \pm 0.059$ (Bonnand et al., 2011). The external reproducibility of NIST SRM 979 is $\delta^{53}Cr = 0.002 \pm 0.026$ (2σ, $n = 20$).

2.4 cGENIE modelling set-up

To estimate the global extent of deoxygenation during the PETM, we compare proxy observations of ocean redox state with model simulations of the Paleogene ocean following the approach described in Monteiro et al. (2012). The model employed was the Earth system model of intermediate complexity cGENIE, a 3D ocean biogeochemical model coupled to a 2D atmospheric model (Ridgwell et al., 2007). Marine productivity is modelled in cGENIE through the activity of both non-fixing phytoplankton and diazotrophs, where productivity is limited by light, temperature and nutrient concentrations of phosphate and fixed nitrogen (nitrate and ammonium)). cGENIE lets nitrogen fixation occur when fixed nitrogen is smaller than a dynamical threshold for oligotrophy which accounts for resource competition. The nitrogen cycle also includes the nitrification process of oxidation of ammonium into nitrate (Monteiro et al., 2012). In the model, denitrification occurs when oxygen concentrations drop below 30 μmol O_2 l^{-1}, which is higher than modern values due to the low model resolution (Monteiro et al., 2012). In cGENIE, the remineralisation of particulate organic matter follows a double exponential decrease with depth which depends on the availability of oxygen, nitrate and sulfate (Ridgwell et al., 2007). Any particulate organic matter reaching the seafloor is instantaneously remineralized into inorganic matter, as no sediments are included in the model. We configured cGENIE for the Eocene using bathymetry and continental configuration derived from the higher resolution model Fast Ocean Atmosphere Model (FOAM) simulations. The annual average wind field transformed to the cGENIE grid came from the Eocene FOAM experiment run with 4x CO_2 (relative to the preindustrial atmospheric value). cGENIE biogeochemistry accounted for carbon, phosphorus, nitrogen, oxygen and sulphur cycling as described by Monteiro et al. (2012), including equations and parameter values for ocean productivity and temperature control.

We ran the model under different environmental forcings, varying the oceanic phosphate inventory and atmospheric CO_2 to investigate the impact of changes in nutrient supply and temperature on oceanic oxygen levels during the PETM. As found in Monteiro et al. (2012), the model shows that ocean oxygen levels at the Eocene were more sensitive to changes in phosphate inventory than changes in atmospheric CO_2 (see supporting information B). The model results are then compared

with published data and data generated in this study for seawater deoxygenation and photic zone euxinia across the PETM (Carmichael et al., 2017; Tables B5 and B6).

We calculate a score of agreement between the model results and data for before and during the PETM (0-1, where 0 indicates no agreement and 1 indicates perfect agreement; Monteiro et al., 2012). Here, we add the distinction between anoxia/suboxia (< 10 µM O_2; Diaz & Rosenberg, 2008) and hypoxia (10-60 µM O_2; Diaz & Rosenberg, 2008; Vaquer-Sunyer & Duarte, 2008) to better capture the subtler deoxygenation that is thought to have taken place during the PETM in comparison to Mesozoic Ocean Anoxic Events (OAEs). The geographical extent of photic zone euxinia has been assessed with a threshold of > 0 µM H_2S (Monteiro et al., 2012). See Supporting Information B for a full description of the agreement calculation.

3. Results

3.1 Chromium and cerium anomalies

DSDP Site 401, located in the North Atlantic, shows a rapid increase in foraminiferal $\delta^{53}Cr$ of about 1.4‰ paired with a decrease in [Cr] of about 1.5 ppm just prior to the CIE (Figure 2). No Cr isotope data are available for the onset of the PETM itself as this was an interval of intense dissolution. This dissolution has led to a condensed section where not enough foraminifera could be obtained for analysis. The highest $\delta^{53}Cr$ values are prior to the onset of the CIE and they recovered to background values 68 kyrs after the CIE onset. Chromium concentrations reach their lowest values of 0.27 ppm prior to the CIE minimum and do not recover within our 400 kyr-record. The severe carbonate dissolution at ODP Site 1263 (Walvis Ridge, South Atlantic), as indicated by a steep drop of ~4.8% in the coarse fraction (CF; all material >63 µm), a monitor of $CaCO_3$ dissolution through this interval, meant that our foraminiferal analysis was unable to capture the onset of the event (Figure 3). While Cr concentrations are highly variable prior to the PETM and after peak-CIE conditions, [Cr] attains its

lowest values during the peak of the CIE. The timing of the crash and recovery in [Cr] corresponds with that of the CF record (Figures 2 and 3).

In the Pacific basin, at ODP Site 1210 (Shatsky Rise) the Cr concentrations are extremely low (down to 0.01 ppm) during the PETM and decrease prior to the CIE. Chromium concentrations are variable prior to the PETM and during the carbon isotope recovery at this site. The maximum δ^{53}Cr value at ODP Site 1210 is 0.71‰ with the highest δ^{53}Cr values occurring approximately 20 kyrs after the onset of the PETM in the middle of the δ^{18}O excursion (Figures 2 and 3). This pattern is unlike the observations at DSDP Site 401, where δ^{53}Cr values shift before the onset of the PETM.

Foraminiferal cerium anomalies of 0.10 – 0.28 (Figure 2) confirm previous findings that the North Pacific Ocean is more oxygenated than the Atlantic Ocean with values at ODP Site 1263 of 0.72 – 1.14 falling within the range found by Zhou et al. (2016). Cerium anomalies of 0.60 – 1.31 at Site 401 suggest that North Atlantic bottom and pore waters were severely hypoxic and potentially anoxic.

3.2 3D Model - data comparison

We reconstructed the change in deoxygenation across the PETM by comparing the data as compiled by Carmichael et al. (2017) (Tables B5 and B6) and results from this study with the cGENIE model results. The best model fit to the data for pre-PETM conditions is achieved with the modern oceanic phosphate inventory (1 x PO_4) and 1-2 times preindustrial atmospheric CO_2 (1-2 x CO_2) (Table B1). The best model fit for the PETM is achieved under 1 x PO_4 and 6 x CO_2 conditions (Table B4; Figure 4) and falls within the estimated pCO_2 for the PETM (e.g. Schubert & Hope Jahren, 2013; Gutjahr et al., 2017). In our model, the Tethys Sea and North Atlantic experience hypoxic to suboxic conditions (Figure 4) even with pre-industrial forcings while significantly less deoxygenation occurs in the Eastern Pacific and Southern Ocean.

4. Discussion

4.1 Global ocean deoxygenation patterns

Our model-data comparison indicates that the Tethys Sea and North Atlantic Ocean both experienced hypoxia to suboxia (Figure 3), even during pre-PETM conditions. While anoxia/suboxia seems to be restricted to the Tethys Sea before and during the PETM, hypoxia spread from the North Atlantic Ocean and some part of the South Atlantic Ocean to the Eastern Pacific Ocean. The Tethys Sea is the only ocean basin which experienced extensive photic-zone euxinia (Figure 4). According to our reconstruction across the PETM, hypoxia rose by 15% to reach 27% of the global ocean volume and anoxia/suboxia rose by 2% to reach 4% of the global ocean volume by varying the CO_2 forcings in the model from 1 to 6 x CO_2 (Table 1).

There is considerable evidence for widespread seafloor anoxia in the Tethys during the PETM (see Carmichael et al. (2017) for a recent compilation; Table 2). Along the northern margins of the Tethys Sea, there is also evidence for persistent photic-zone euxinia (e.g. Dickson et al., 2014) and intermittent euxinia along the southern and eastern margins during the PETM (Carmichael et al., 2017). The highly reduced state of the Tethys Sea during the PETM is captured by our model-data comparison which also indicates the presence of strong photic-zone euxinia in the Eastern Tethys (Figure 4). Our model-data comparison also suggests that low-oxygen environments were present in the Tethys Sea prior to the PETM. Due to its restricted water exchange and relative proximity to land, the Tethys Sea could have acted as a trap for nutrients causing high productivity leading to anoxic to euxinic conditions (Carmichael et al., 2017).

In contrast to the Tethys Sea, the Atlantic Ocean was more oxygenated before and during the PETM (Figure 4). Regionally, the North Atlantic was already hypoxic prior to the PETM whereas the South Atlantic was mostly oxic representing the more restricted North Atlantic versus the more oxygenated South Atlantic due to the proposed location of bottom water formation (Tripati & Elderfield, 2005).

353 Neodymium isotope data suggest that there was limited water exchange between the North and South
354 Atlantic (Abbott et al., 2016).
355
356 Our model-data comparison indicates that the Pacific Ocean was well-oxygenated prior to the PETM,
357 except for the area off the western coast of South America (Figure 4), where analogous to today, the
358 deflection of waters would have resulted in upwelling, nutrient enrichment and high productivity.
359 However, in agreement with Cr isotope data, our model runs shows wide-spread reductions in
360 dissolved oxygen content to hypoxic levels in the East Pacific during the PETM. This challenges the
361 idea that the PETM was geographically substantially less widespread than the Mesozoic Ocean
362 Anoxic Events (OAEs; Carmichael et al., 2017), although the overall decrease in oxygen
363 concentrations is modest in comparison to, e.g., OAE 2 (Monteiro et al., 2012).
364
365 Our Cr isotope and concentration records are different both stratigraphically and in excursion size at
366 the three sites and suggest a local redox control. Therefore, variations in δ^{53}Cr values do not
367 necessarily represent a global signal. We suggest that a range of mechanisms were responsible for the
368 differences in the δ^{53}Cr records between the sites, which we will explore in further detail in the
369 following sections.
370
371 Published seawater data shows that modern seawater δ^{53}Cr measurements are distributed within the
372 range of 0.1-1.8‰ with a median value of 1.2‰ (Bonnand et al., 2013; Scheiderich et al., 2015;
373 Economou-Eliopoulos et al., 2015; Pereira et al., 2016; Paulukat et al., 2016; Holmden et al., 2016;
374 Goring-Harford et al., 2018). Open ocean intermediate and deep waters have a relatively constant
375 δ^{53}Cr signature (Goring-Harford et al., 2018). Less oxygenated waters are expected to have a heavier
376 δ^{53}Cr due to partial isotopic fractionation under more reducing conditions (Ellis et al., 2002).
377 Therefore, one may expect intermediate and deep water δ^{53}Cr to reflect changes in redox state which
378 should be reflected by foraminiferal calcite (Goring-Harford et al., 2018; Remmelzwaal et al., in
379 review). The δ^{53}Cr values for the PETM at ODP Site 1210 fall within the oxic and hypoxic range
380 (Goring-Harford et al., 2018). Peak Cr isotope values at DSDP Site 401 and ODP Site 1263 are higher

than the modern range for oxic and hypoxic seawater. We assume this implies that ODP Site 1263 and DSDP 401 might yield Cr isotope values that can be interpreted as reflecting hypoxic-anoxic conditions during the PETM, whereas the Pacific recorded minor deoxygenation within the upper bounds of modern oxic seawater. These findings are consistent with Ce anomalies which suggest the North Pacific remained oxic in contrast to the North and South Atlantic (Figure 2).

4.2 Deoxygenation through ocean circulation changes

A switch to warmer, more corrosive and less oxygenated intermediate waters at Walvis Ridge in the South Atlantic, as postulated by Lunt et al. (2010) can explain the correlation between δ^{53}Cr, [Cr], and the CF record at ODP Site 1263 (generated for this study and in agreement with the higher-resolution CF record by Kelly et al. (2010)), and the intensified carbonate dissolution this represents (Figure 3). While there is no agreement about the circulation switch (e.g. Nunes & Norris, 2006; Alexander et al., 2015), it is thought that during the latest Palaeocene, deep ocean formation in the Southern Ocean decreased while a new circulation cell developed in the North Pacific (Tripati & Elderfield, 2005). During the PETM an abrupt switch to North Pacific convection and a salinity-stratified ocean occurred leading to substantial warming of intermediate and deep waters (Tripati & Elderfield, 2005; Lunt et al., 2010). Additional evidence for fundamental changes in intermediate and deep-water circulation during the latest Palaeocene and PETM comes from Nd isotopes that suggest changes in deep-water circulation started prior to PETM warmth (Abbott et al., 2016). Model simulations of bottom water circulation during the PETM show that corrosive bottom waters built up in the North Atlantic and flowed to the South Atlantic during the PETM (Alexander et al., 2015). This is, however, in disagreement with the Nd isotope data, which suggests a more limited exchange of waters between ocean basins (Abbott et al., 2016). The warming of South Atlantic intermediate and deep waters would trigger a reduction in oxygen concentrations and could provide an explanation for the response in Cr isotopes. The extraordinarily high δ^{53}Cr at ODP Site 1263 (~ +3.5‰) can be partly attributed to partial reduction associated with the expansion of a major oxygen minimum zone off the West-African coast into intermediate waters as suggested by Mn and U enrichment factors (EF; Chun et al.,

2010). Unlike the Mn_{EF} and U_{EF} at ODP Site 1263 (Chun et al., 2010) and our Ce/Ce* results (Figure 2), the $\delta^{53}Cr$ record at Site 1263 does not provide any evidence for hypoxia prior to or after the CIE (Figure 2) leaving open questions and disagreement with previous studies (Chun et al., 2010; Pälike et al., 2014; Zhou et al., 2016). This potentially signifies that Cr and Ce have different oxygen concentration thresholds to Mn and U below which these become redox-reactive. This is partially captured by different standard reduction potentials at seawater pH levels for Cr, Ce Mn, and U (Brookins, 1988).

The Ce/Ce* at ODP Site 1263 peaks when our measured $\delta^{53}Cr$ values are highest, around 40 kyrs after the onset of the PETM, and subsequently recovers to values indicative of near oxic conditions. The Ce/Ce* record at ODP Site 1263 by Zhou et al. (2016) also peaks approximately 35 kyrs after the CIE at anoxic values. However, our foraminiferal cerium anomalies show a clearer pattern of decreasing oxygen levels prior to the PETM and a recovery afterwards than the Ce/Ce* from fish teeth, although the latter are recorded throughout the PETM unlike the foraminiferal data due to carbonate dissolution (Zhou et al., 2016). Geochemical evidence exists for oxic conditions at the nearby deeper ODP Site 1262 (Chun et al., 2010; Zhou et al., 2016), although it is thought transient hypoxia did occur in the carbonate-free interval at ODP Site 1262 (Post et al., 2016). This suggests that deoxygenation mainly occurred at intermediate depths in the South Atlantic, and less so deeper in the water column.

Our model-data comparison and Cr isotope data support oxic bottom water conditions before the PETM at ODP Site 1263 in the South Atlantic (Figure 4) in line with a more intense deep convection in the Southern Ocean prior to and after the PETM (Tripati & Elderfield, 2005; Nunes & Norris, 2006; Lunt et al., 2010). Hosing experiments in two climate models (CCSM3 and GENIE) show that stratification can lead to a severe loss of oxygen in the South Atlantic and Indian Oceans (Zhou et al., 2016). Oxic conditions before the PETM are consistent with our Cr isotope data and recent magnetofossil data (Chang et al., 2018) but are in disagreement with trace metal geochemical data

(Chun et al., 2010; Pälike et al., 2014; and Zhou et al., 2016). A difference in standard reduction potentials between CrO_4^{2-}, MnO_2, Ce^{4+} and $UO_2(CO_3)_3^{4-}$ may cause this apparent discrepancy.

The smaller magnitude of the $\delta^{53}Cr$ excursion at ODP Site 1210 compared to the other sites (Figure 2) indicates less intense deoxygenation in the subtropical Pacific gyre than in the Atlantic Ocean. The oligotrophic environment, which would have been increased due to higher stratification during the PETM compared to background, in combination with the position of the $\delta^{53}Cr$ peak within the acme of warming indicated by benthic $\delta^{18}O$ (Zachos et al., 2003; Tripati & Elderfield, 2005) suggests the $\delta^{53}Cr$ anomaly can be attributed mainly to ocean warming driving decreased oxygen solubility. Our model-data reconstruction also suggests that deoxygenation across the PETM was due to warming resulting from a 3 to 6-fold increase in atmospheric CO_2. It must be noted that alternatively the model is very sensitive to nutrient fluxes and therefore only a small increase in nutrient run-off would create a similar effect. This interpretation would support studies showing increases in weathering (e.g. Ravizza et al., 2001; Gavrilov et al., 2003; John et al., 2008; Dickson et al., 2015) although it is not clear whether the increased run-off, increasing productivity in coastal sites, made it out into the open ocean (e.g. Gibbs et al., 2006; Carmichael et al., 2017). The switch to North Pacific deep-water formation as discussed earlier can explain the more pronounced change in [Cr] than in $\delta^{53}Cr$ during the CIE due to a decreased transport of Cr to the open ocean. Mn_{EF} and U_{EF} support the observation from $\delta^{53}Cr$ and Ce/Ce* that Pacific intermediate waters remained oxic (Pälike et al., 2014). The recovery in $\delta^{53}Cr$ at ODP Site 1210 was rapid as intermediate waters cool.

4.3 Evolution of deoxygenation

To pinpoint a source for the introduction of reduced carbon during the PETM it is imperative to assess the timing of deoxygenation occurring at each of the sites. In the Bay of Biscay (DSDP 401), near the proposed site of biogenic methane injection and volcanism, $\delta^{53}Cr$ values become more positive prior to the CIE and peak 9,000 years before the onset of the PETM (Figure 2a) and are corroborated by a drop in Cr concentrations. Ce/Ce* attain anoxic values (Ce/Ce* > 1) at the same time approximately

9,000 years before the onset of the PETM (Figure 2c). It is possible that sediments deposited just prior to the PETM at DSDP Site 401 may have been influenced by interstitial fluid flow during the PETM which could also partially explain why the redox response at this location occurred prior to the PETM. However, there is currently no sedimentological evidence to support this. Chromium isotope values in the Pacific (ODP Site 1210) peak 20 kyrs after the CIE onset, during maximum warmth (McCarren et al., 2008; Figure 2a). The timing of deoxygenation and response of $\delta^{53}Cr$ at Walvis Ridge cannot be determined due to the severe carbonate dissolution during the onset and main body of the PETM at this site. However, fish teeth Ce/Ce* data from Zhou et al. (2016) along with foraminiferal Ce/Ce* from this study suggest peak anoxia in the South Atlantic occurred approximately 35 - 45 kyrs after the onset of the PETM. Importantly, deoxygenation in the Pacific occurred before that in the South Atlantic as shown by $\delta^{53}Cr$ at ODP Site 1210 on Shatsky Rise in the North Pacific (Figure 2) and Ce/Ce* at ODP Site 1263 on Walvis Ridge in the South Atlantic (Chun et al., 2010; Zhou et al., 2016) making the interpretation of a dissipation of the signal due to circulation impossible. Our model-data comparison reinforces previous suggestions that anoxia developed more easily in the Tethys Sea and Atlantic Ocean than in the Pacific Ocean during the PETM (Chun et al., 2010; Pälike et al., 2014; Zhou et al., 2016) with conditions of anoxia and hypoxia present in these basins even under pre-PETM conditions. However, our model-data comparison (Figure 4) shows that during the PETM the Pacific Ocean experienced some deoxygenation reaching oxic-hypoxic conditions in the North Pacific Ocean and hypoxia in the eastern Pacific Ocean.

4.4 Temperature control on open ocean deoxygenation

Comparing the maximum observed excursion size in $\delta^{53}Cr$ during the PETM against the maximum carbon and benthic oxygen isotope excursions (CIE and OIE, respectively) illustrates that the size of the carbon cycle perturbation does not appear to have an impact on the size of the observed $\delta^{53}Cr$ excursion (Figures 2 and 3). In contrast, a positive correlation is found with the magnitude of the benthic OIE, implying that warming exerts significant control on the size of the $\delta^{53}Cr$ perturbation and by extrapolation over the expansion of open ocean low-oxygen environments during the Late

492 Palaeocene – Early Eocene. As the $\delta^{53}Cr$ records are incomplete for ODP sites 401 and 1263, these
493 correlations need to be approached with caution and may underestimate the Cr excursion.
494 Additionally, when considering vital effects, the shifts in the foraminiferal $\delta^{53}Cr$ likely slightly
495 overestimate environmental changes (Remmelzwaal et al., in review), since the maximum test size of
496 planktic foraminifera may have increased by up to 150 µm during the PETM depending on the
497 foraminiferal species although overall decreases in test size have also been reported (Kaiho et al.,
498 2006; Petrizzo, 2007; Alegret et al., 2010). Based on Remmelzwaal et al. (in review), the change in
499 $\delta^{53}Cr$ composition associated with the increase in foraminiferal test size and assemblage could
500 account for a maximum of +0.1‰ to +0.3‰ of the Cr isotope signal during the PETM depending on
501 the test shape if a test increase is assumed. However, size changes in the foraminiferal assemblage
502 have not yet been quantified. These factors affecting Cr isotopes do not impede converting the
503 benthic OIE into temperature-associated dissolved oxygen loss (Broeker & Peng, 1982). This shows
504 that thermal effects account for a loss of -13.0 to -32.7 µmol/kg O_2 at the study sites which by itself is
505 not enough to produce hypoxia. Warming will have additionally increased microbial metabolic rates
506 (Pörtner et al., 2014). It has been suggested that the open ocean experienced increased oligotrophy
507 during the PETM (Gibbs et al., 2006). This, however, would not necessarily imply less biological and
508 biogeochemical activity (Ma et al., 2014). In combination with increased metabolic rates and more
509 extensive remineralisation, a constant or even decreasing primary productivity in the open ocean
510 could have resulted in amplifying deoxygenation associated with warming of the ocean through
511 increased export productivity. We suggest that warming of intermediate waters was one of the
512 principal drivers of deoxygenation during the PETM with the scale of warming (~5 degrees Celsius;
513 Dunkley-Jones et al., 2013) producing wide-spread hypoxia throughout the North and South Atlantic.
514 Our findings align with modern observations that warming is a major controlling factor on open ocean
515 deoxygenation (Schmidtko et al., 2017). The extent of deoxygenation during the PETM shows that
516 rapid temperature increases have caused wide-spread open ocean hypoxia in the past and that future
517 oceans may also experience wide-spread deoxygenation due to anthropogenic global warming.
518

519 **5. Conclusions**

This study shows that foraminiferal $\delta^{53}Cr$ during the Late Paleocene and Early Eocene is controlled by local factors contributing to seawater deoxygenation, which is in line with the heterogeneity of Cr in modern oceans and its comparatively short residence time. Our model output indicates that deoxygenation was widespread throughout the global oceans during the PETM, while our Cr datasets add valuable information on local variation in bottom water deoxygenation. We attribute the deoxygenation mainly to rising temperatures in intermediate ocean waters due to higher atmospheric CO_2, based on an apparent correlation between the magnitude of the benthic oxygen isotope and the Cr isotope excursions. Warmer intermediate waters, an increased microbial loop and remineralisation, and declines in oxygen solubility jointly are suggested to have caused the lower oxygen concentrations. If any geographical spreading of deoxygenation occurred, it appears to have originated in the North Atlantic (DSDP Site 401), in line with evidence for this basin having been proximal to the location of injection of reduced carbon (Svensen et al., 2004). Chromium isotope values and Ce anomalies at ODP Site 1210 indicate this site may have been less impacted by deoxygenation than the two Atlantic sites.

6. Acknowledgements

This work was supported by NERC studentship 1509236 awarded to SR and NERC grant NE/H006443/1 awarded to RHJ, IJP and CP; the Wolfson Research Merit Award from the Royal Society to DNS; and by NERC research fellowship NE/J019062/1 awarded to FMM. The authors would like to express their gratitude to Kirsty Edgar, Sam Hammond, Sarah Greene and Richard Pancost for their invaluable help and would like to thank Richard Norris and the International Ocean Discovery Program for sharing samples. Data supporting the conclusions of this study can be found in the Supporting Information.

7. References

548 Abbott, A. N., Haley, B. A., Tripati, A. K., & Frank, M. (2016). Constraints on ocean circulation at
549 the Paleocene-Eocene Thermal Maximum from neodymium isotopes. *Climate of the Past*, 12, 837-
550 847. https://doi.org/10.5194/cp-12-837-2016

551

552 Alegret, L., Ortiz, S., Arenillas, I., & Molina, E. (2010). What happens when the ocean is overheated?
553 The foraminiferal response across the Paleocene-Eocene Thermal Maximum at the Alamedilla section
554 (Spain). *GSA Bulletin*, 122, 1616-1624. https://doi.org/10.1130/B30055.1

555

556 Alexander, K., Meissner, & K. J., Bralower, T. J. (2015). Sudden spreading of corrosive bottom water
557 during the Palaeocene-Eocene Thermal Maximum. *Nature Geoscience*, 8, 458-461.
558 https://doi.org/10.1038/ngeo2430

559

560 Barker, S., Greaves, M., & Elderfield, H. (2003). A study of cleaning procedures used for
561 foraminiferal Mg/Ca paleothermometry. *Geochemistry, Geophysics, Geosystems*, 4, 8407.
562 https://doi.org/10.1029/2003GC000559

563

564 Bice, K. L., & Marotzke, J. (2002). Could changing ocean circulation have destabilized methane
565 hydrate at the Paleocene/Eocene boundary? *Paleoceanography*, 17, 1018.
566 https://doi.org/10.1029/2001PA000678

567

568 Bonnand, P., Parkinson, I. J., James, R. H., Karjalainen, A.-M., & Fehr, M. A. (2011). Accurate and
569 precise determination of stable Cr isotope compositions in carbonates by double spike MC-ICP-MS.
570 *Journal of Analytical Atomic Spectrometry*, 26, 528-535. https://doi.org/10.1039/c0ja00167h

571

572 Bonnand, P., James, R. H., Parkinson, I. J., Connelly, D. P., & Fairchild, I. J. (2013). The chromium
573 isotopic composition of seawater and marine carbonates. *Earth and Planetary Science Letters*, 382,
574 10-20. https://doi.org/10.1016/j.epsl.2013.09.001

Bornemann, A., Norris, R. D., Lyman, J. A., D'haenens, S., Groeneveld, J., Rohl, U., et al. (2014). Persistent environmental change after the Paleocene-Eocene Thermal Maximum in the eastern North Atlantic. *Earth and Planetary Science Letters*, 394, 70-81. https://doi.org/10.1016/j.epsl.2014.03.017

Brookins, D. G. (1988). *Eh-pH Diagrams for Geochemistry.* Berlin, Heidelberg: Springer-Verlag.

Carmichael, M. J., Inglis, G. N., Badger, M. P. S., Naafs, B. D. A., Behrooz, L., Remmelzwaal, S., et al. (2017). Hydrological and associated biogeochemical consequences of rapid global warming during the Paleocene-Eocene Thermal Maximum. *Global and Planetary Change*, 157, 114-138. https://doi.org/10.1016/j.gloplacha.2017.07.014

Chang, L., Harrison, R. J., Zeng, F., Berndt, T. A., Roberts, A. P., Heslop, D., et al. (2018). Coupled microbial bloom and oxygenation decline recorded by magnetofossils during the Palaeocene-Eocene Thermal Maximum. *Nature Communications*, 9. https://doi.org/10.1038/s41467-018-06472-y

Chun, C. O. J., Delaney, M. L., & Zachos, J. C. (2010). Paleoredox changes across the Paleocene-Eocene thermal maximum, Walvis Ridge (ODP Sites 1262, 1263, and 1266): Evidence from Mn and U enrichment factors. *Paleoceanography*, 25, PA4202. https://doi.org/10.1029/2009PA001861

Colosimo, A. B., Bralower, T. J., & Zachos, J. C. (2006). Evidence for lysocline shoaling at the Paleocene/Eocene Thermal Maximum on Shatsky Rise, northwest Pacific. In: Bralower, T. J., Premoli Silva, Malone M. J. (Eds.), 2006. *Proceedings of the Ocean Drilling Program, Scientific Results*, 198: College Station, TX (Ocean Drilling Program).

Cramer, B. S., Wright, J. D., Kent, D. V., & Aubry, M.-P. (2003). Orbital climate forcing of $\delta^{13}C$ excursions in the late Paleocene–early Eocene (chrons C24n–C25n), *Paleoceanography*, 18, 1097. https://doi.org/10.1029/2003PA000909

Cranston, R. E., & Murray, J. W. (1980). Chromium species in the Columbia River and Estuary. *Limnology and Oceanography*, 25, 1104-1112. https://doi.org/10.4319/lo.1980.25.6.1104

De Baar, H. J. W., German, C. R., Elderfield, H., & Vangaans, P. (1988). Rare-earth element distributions in anoxic waters of the Cariaco Trench. *Geochimica et Cosmochimica Acta*, 52, 1203-1219. https://doi.org/10.1016/0016-7037(88)90275-X

Diaz, R. J., & Rosenberg, R. (2008). Spreading dead zones and consequences for marine ecosystems. *Science*, 321, 926-929. https://doi.org/ 10.1126/science.1156401

Dickson, A. J., Cohen, A. S., & Coe, A. L. (2012). Seawater oxygenation during the Paleocene-Eocene Thermal Maximum. *Geology*, 40, 639-642. https://doi.org/10.1130/G32977.1

Dickson, A. J., Cohen, A. S., & Coe, A. L. (2014). Continental margin molybdenum isotope signatures from the early Eocene. *Earth and Planetary Science Letters*, 404, 389-395. https://doi.org/10.1016/j.epsl.2014.08.004

Dickson, A. J., Cohen, A. S., Coe, A. L., Davies, M., Shcherbinina, E. A., & Gavrilov, Y. O. (2015). Evidence for weathering and volcanism during the PETM from Arctic Ocean and Peri-Tethys osmium isotope records. *Palaeogeography, Palaeoclimatology, Palaeoecology*, 438, 300-307. https://doi.org/10.1016/j.palaeo.2015.08.019

Dunkley-Jones, T., Lunt, D. J., Schmidt, D. N., Ridgwell, A., Sluijs, A., Valdes, P. J., & Maslin, M. (2013). Climate model and proxy data constraints on ocean warming across the Paleocene-Eocene Thermal Maximum. *Earth-Science Reviews*, 125, 123-145. https://doi.org/10.1016/j.earscirev.2013.07.004

631 Economou-Eliopoulos, M., Frei, R., & Megremi, I. (2016). Potential leaching of Cr(VI) from laterite
632 mines and residues of metallurgical products (red mud and slag): an integrated approach. *Journal of*
633 *Geochemical Exploration*, 162, 40-49. https://doi.org/10.1016/j.gexplo.2015.12.007
634
635 Ellis, A. S., Johnson, T. M., & Bullen, T. D. (2002). Chromium isotopes and the fate of hexavalent
636 chromium in the environment. *Science*, 295, 2060-2062. https://doi.org/ 10.1126/science.1068368
637
638 Gavrilov, Y., Shcherbina, E. A., & Oberhänsli, H. (2003). Paleocene-Eocene boundary events in the
639 northeastern Peri-Tethys, in Wing, S.L., et al., eds., Causes and consequences of globally warm
640 climates in the early Paleogene: *Geological Society of America Special Paper*, 369, 147-168.
641
642 Gibbs, S. J., Bralower, T. J., Bown, P. R., Zachos, J. C., & Bybell, L. M. (2006). Shelf and open-
643 ocean calcareous phytoplankton assemblages across the Paleocene-Eocene Thermal Maximum:
644 Implication for global productivity gradients. *Geology*, 34, 233-236. https://doi.org/10.1130/G22381.1
645
646 Goring-Harford, H. J., James, R. H., Pearce, C. R., Connelly, D. P., Klar, J. K., & Parkinson, I. J.
647 (2017). On the Cr isotopic composition of seawater. *Goldschmidt Abstracts*, 2017.
648
649 Goring-Harford, H., Klar, J. K, Pearce, C. R., Connelly, D. P., Achterberg, E. P., & James, R. H.
650 (2018). Behaviour of chromium isotopes in the eastern sub-tropical Atlantic Oxygen Minimum Zone.
651 *Geochimica et Cosmochimica Acta* (In press). https://doi.org/10.1016/j.gca.2018.03.004
652
653 Gutjahr, M., Ridgwell, A., Sexton, P. F., Anagnostou, E., Pearson, P. N., Pälike, H., et al. (2017).
654 Very large release of mostly volcanic carbon during the Palaeocene-Eocene Thermal Maximum.
655 *Nature*, 548, 573-577. https://doi.org/ 10.1038/nature23646
656

Haley, B. A., Klinkhammer, G. P., & McManus, J. (2004). Rare earth elements in pore waters of marine sediments. *Geochimica et Cosmochimica Acta*, 68, 1265-1279. https://doi.org/10.1016/j.gca.2003.09.012

Hein, J. R., & Koschinsky, A. (2014). Deep-Ocean Ferromanganese Crusts and Nodules. In H. D. Holland & K. K. Turekian (Eds.), *Treatise on Geochemistry* (Second Edition, pp. 273-291). Oxford: Elsevier. https://doi.org/10.1016/B978-0-08-095975-7.01111-6

Holmden, C., Jacobson, A., Sageman, B., & Hurtgen, M. (2016). Response of the Cr isotope proxy to Cretaceous Ocean Anoxic Event 2 in a pelagic carbonate succession from the Western Interior Seaway. *Geochimica et Cosmochimica Acta*, 186, 277-295. https://doi.org/10.1016/j.gca.2016.04.039

John, C. M., Bohaty, S. M., Zachos, J. C., Sluijs, A., Gibbs, S., Brinkhuis, H., & Bralower, T. J. (2008). North American continental margin records of the Paleocene-Eocene thermal maximum: Implications for global carbon and hydrological cycling. *Paleoceanography*, 23, PA2217. https://doi.org/10.1029/2007PA001465

Kaiho, K., Takeda, K., Petrizzo, M. R., & Zachos, J. C. (2006). Anomalous shifts in tropical Pacific planktonic and benthic foraminiferal test size during the Paleocene-Eocene thermal maximum. *Palaeogeography, Palaeoclimatology, Palaeoecology*, 237, 456-464. https://doi.org/10.1016/j.palaeo.2005.12.017

Keeling, R. F., Körtzinger, A., & Gruber, N. (2010). Ocean deoxygenation in a warming world. *Annual Reviews of Marine Science*, 2, 199-229. https://doi.org/10.1146/annurev.marine.010908.163855

Kelly, D. C., Zachos, J. C., Bralower, T. J., & Schellenberg, S. A. (2005). Enhanced terrestrial weathering/runoff and surface ocean carbonate production during the recovery stages of the

685 Paleocene-Eocene thermal maximum. *Paleoceanography*, 20, PA4023. https://doi.org/
686 10.1029/2005PA001163
687
688 Kelly, D. C., Nielsen, T. M. J., McCarren, H. K., Zachos, J. C., & Röhl, U. (2010). Spatiotemporal
689 patterns of carbonate sedimentation in the South Atlantic: Implications for carbon cycling during the
690 Paleocene-Eocene thermal maximum. *Palaeogeography, Palaeoclimatology, Palaeoecology*, 293, 30-
691 40. https://doi.org/10.1016/j.palaeo.2010.04.027
692
693 Laskar, J., Fienga, A., Gastineau, M., & Manche, H. (2011). La2010: A new orbital solution for the
694 long-term motion of the Earth. *Astronomy and Astrophysics*, 532, A89. https://doi.org/10.1051/0004-
695 6361/201116836
696
697 Lunt, D. J., Valdes, P. J., Dunkley Jones, T., Ridgwell, A., Haywood, A. M., Schmidt, D. N., et al.
698 (2010). CO_2-driven ocean circulation changes as an amplifier of Paleocene-Eocene thermal maximum
699 hydrate destabilization. *Geology*, 38, 875-878. https://doi.org/10.1130/G31184.1
700
701 Ma, Z., Gray, E., Thomas, E., Murphy, B., Zachos, J., & Paytan, A. (2014). Carbon sequestration
702 during the Palaeocene-Eocene Thermal Maximum by an efficient biological pump. *Nature*
703 *Geoscience*, 7, 382-388. https://doi.org/ 10.1038/ngeo2139
704
705 McCarren, H., Thomas, E., Hasegawa, T., Röhl, U., & Zachos, J. C. (2008). Depth dependency of the
706 Paleocene-Eocene carbon isotope excursion: Paired benthic and terrestrial biomarker records (ocean
707 drilling program leg 208, Walvis Ridge). *Geochemistry, Geophysics, Geosystems*, 9, Q10008.
708 https://doi.org/10.1029/2008GC002116
709
710 Monteiro, F. M., Pancost, R. D., Ridgwell, A., & Donnadieu, Y. (2012). Nutrients as the dominant
711 control on the spread of anoxia and euxinia across the Cenomanian-Turonian oceanic anoxic event

712 (OAE2): Model-data comparison. *Paleoceanography*, 27, PA4209.
713 https://doi.org/10.1029/2012PA002351
714
715 Nicolo, M. J., Dickens, G. R., & Hollis, C. J. (2010). South Pacific intermediate water oxygen
716 depletion at the onset of the Paleocene-Eocene thermal maximum as depicted in New Zealand margin
717 sections. *Paleoceanography*, 25, PA4210. https://doi.org/10.1029/2009PA001904
718
719 Nunes, F., & Norris, R. D. (2006). Abrupt reversal in ocean overturning during the
720 Palaeocene/Eocene warm period. *Nature*, 439, 60-63. htpps://doi.org/ 10.1038/nature04386
721
722 Pälike, C., Delaney, M. L., & Zachos, J. C. (2014). Deep-sea redox across the Paleocene-Eocene
723 thermal maximum. *Geochemistry, Geophysics, Geosystems*, 15, 1038-1053.
724 https://doi.org/10.1002/2013GC005074
725
726 Palmer, M. R. (1985). Rare earth elements in foraminifera tests. *Earth and Planetary Science Letters*,
727 73, 285-298. https://doi.org/10.1016/0012-821X(85)90077-9
728
729 Pardo, A., Keller, G., Molina, E., & Canudo, J. (1997). Planktic foraminiferal turnover across the
730 Paleocene-Eocene transition at DSDP Site 401, Bay of Biscay, North Atlantic. Marine
731 Micropaleontology, 29, 129-158. https://doi.org/10.1016/S0377-8398(96)00035-7
732
733 Paulukat, C., Gilleaudeau, G. J., Chernyavskiy, P., & Frei, R. (2016). The Cr-isotope signature of
734 surface seawater: a global perspective. *Chemical Geology*, 444, 101-109.
735 https://doi.org/10.1016/j.chemgeo.2016.10.004
736
737 Penman, D. E., Hönisch, B., Zeebe, R. E., Thomas, E., & Zachos, J. C. (2014). Rapid and sustained
738 surface ocean acidification during the Paleocene-Eocene Thermal Maximum. *Paleoceanography*, 29,
739 357–369. https://doi.org/10.1002/2014PA002621

Penman, D. E., Turner, S. K., Sexton, P. F., Norris, R. D., Dickson, A. J., Boulila, S., et al. (2016). An abyssal carbonate compensation depth overshoot in the aftermath of the Palaeocene–Eocene Thermal Maximum. *Nature Geoscience*, 9, 575–580. https://doi.org/10.1038/ngeo2757

Pereira, N. S., Voegelin, A. R., Paulukat, C., Sial, A. N., Ferreira, V. P., & Frei, R. (2016). Chromium-isotope signatures in scleractinian corals from the Rocas Atoll, tropical South Atlantic. *Geobiology*, 14, 1009-1023. https://doi.org/10.1111/gbi.12155

Petrizzo, M. R. (2007). The onset of the Paleocene-Eocene Thermal Maximum (PETM) at Sites 1209 and 1210 (Shatsky Rise, Pacific Ocean) as recorded by planktonic foraminifera. Marine Micropaleontology, 63, 187-200. https://doi.org/10.1016/j.marmicro.2006.11.007

Pörtner, H. O., Karl, D., Boyd, P. W., Cheung, W., Lluch-Cota, S. E., Nojiri, Y., et al., (Eds.) (2014). Climate Change 2014: Impacts, Adaptation, and Vulnerability. Part A: Global and Sectoral Aspects. *Contribution of Working Group II to the Fifth Assessment Report of the Intergovernmental Panel on Climate Change*. Cambridge University Press, Cambridge, United Kingdom and New York, NY, USA, 411-484.

Post, J. E., Thomas, E., & Heaney, P. J. (2016). Jianshuiite in oceanic manganese nodules at the Paleocene-Eocene boundary. *American Mineralogist* 101, 407-414. https://doi.org/10.2138/am-2016-5347

Qin, L., & Wang, X. (2017). Chromium Isotope Geochemistry. *Reviews in Mineralogy & Geochemistry*, 82, 379-414. https://doi.org/10.2138/rmg.2017.82.10

766 Ravizza, G., Norris, R. N., Blusztajn, J., & Aubry, M.-P. (2001). An osmium isotope excursion
767 associated with the late Paleocene thermal maximum: evidence of intensified chemical weathering.
768 *Paleoceanography*, 16, 155-163. https://doi.org/10.1029/2000PA000541
769
770 Reinhard, C. T., Planavsky, N. J., Wang, X., Fischer, W. W., Johnson, T. M., & Lyons, T. W. (2014).
771 The isotopic composition of authigenic chromium in anoxic marine sediments: A case study from the
772 Cariaco basin. *Earth and Planetary Science Letters*, 407, 9-18.
773 https://doi.org/10.1016/j.epsl.2014.09.024
774
775 Remmelzwaal., S. R. C., Sadekov, A. Y., Parkinson, I. J., Schmidt, D. N., Titelboim, D., Abramovich,
776 S., et al. (in review). Post-depositional overprinting of chromium in foraminifera. *Earth and Planetary*
777 *Science Letters*.
778
779 Ridgwell, A., Hargreaves, J. C., Edwards, N. R., Annan, J. D., Lenton, T. M., Marsh, R., et al. (2007).
780 Marine geochemical data assimilation in an efficient Earth System Model of global biogeochemical
781 cycling. *Biogeosciences*, 4, 87-104. https://doi.org/10.5194/bg-4-87-2007
782
783 Röhl, U., Westerhold, T., Bralower, T. J., & Zachos, J. C. (2007). On the duration of the Paleocene-
784 Eocene thermal maximum (PETM). *Geochemistry Geophysics Geosystems*, 8, Q12002.
785 https://doi.org/10.1029/2007GC001784
786
787 Scheiderich, K., Amini, M., Holmden, C., & Francois, R. (2015). Global variability of chromium
788 isotopes in seawater demonstrated by Pacific, Atlantic, and Arctic Ocean samples. *Earth and*
789 *Planetary Science Letters*, 423, 87-97. https://doi.org/10.1016/j.epsl.2015.04.030
790
791 Schmidtko, S., Stramma, L., & Visbeck, M. (2017). Decline in global oceanic oxygen content during
792 the past five decades. *Nature*, 542, 335–339. https://doi.org/10.1038/nature21399
793

794 Svensen, H., Planke, S., Malthe-Sørenssen, A., Jamtveit, B., Myklebust, R., Eidem, T. R., & Rey, S.
795 S. (2004). Release of methane from a volcanic basin as a mechanism for initial Eocene global
796 warming. *Nature*, 429, 542-545. htpps://doi.org/10.1038/nature02566
797
798 Tang, Y., Elzinga, E. J., Lee, Y. J., & Reeder, R. J. (2007). Coprecipitation of chromate with calcite:
799 Batch experiments and X-ray absorption spectroscopy. *Geochimica et Cosmochimica Acta*, 71, 1480-
800 1493. https://doi.org/10.1016/j.gca.2006.12.010
801
802 Taylor, S. R., & McLennan, S. M. (1985). The Continental Crust: Its Composition and Evolution.
803 Blackwell Scientific.
804
805 Tostevin, R., Shields, G. A., Tarbuck, G. M., He, T., Clarkson, M. O., & Wood, R. A. (2016).
806 Effective use of cerium anomalies as a redox proxy in carbonate-dominated marine settings. *Chemical*
807 *Geology*, 438, 146-162. https://doi.org/10.1016/j.chemgeo.2016.06.027
808
809 Tremolada, F., & Bralower, T. J. (2004). Nannofossil assemblage fluctuations during the Paleocene–
810 Eocene Thermal Maximum at Sites 213 (Indian Ocean) and 401 (North Atlantic Ocean):
811 palaeoceanographic implications. *Marine Micropaleontology*, 52, 107-116.
812 https://doi.org/10.1016/j.marmicro.2004.04.002
813
814 Tripati, A., & Elderfield, H. (2005). Deep-sea temperature and circulation changes at the Paleocene-
815 Eocene Thermal Maximum. *Science*, 308, 1894-1898. https://doi.org/ 10.1126/science.1109202
816
817 Vaquer-Sunyer, R., & Duarte, C. M. (2008). Thresholds of hypoxia for marine biodiversity.
818 *Proceedings of the National Academy of Sciences*, 105, 15452-15457.
819 https://doi.org/10.1073/pnas.0803833105
820

821 Wang, X., Reinhard, C. T., Planavsky, N. J., Owens, J. D., Lyons, T. W., & Johnson, T. M. (2016).
822 Sedimentary chromium isotopic compositions across the Cretaceous OAE2 at Demerara Rise Site
823 1258. *Chemical Geology*, 429, 85-92. https://doi.org/10.1016/j.chemgeo.2016.03.006
824
825 Wang, X., Planavsky, N. J., Hull, P. M., Tripati, A. E., Zou, H. J., Elder, L., Henehan, M. (2017).
826 Chromium isotopic composition of core-top planktonic foraminifera. *Geobiology*, 15, 51-64.
827 https://doi.org/10.1111/gbi.12198
828
829 Westerhold, T., Röhl, U., Raffi, I., Fornaciari, E., Monechi, S., Reale, V., et al. (2008). Astronomical
830 calibration of the Paleocene time. *Palaeogeography, Palaeoclimatology, Palaeoecology*, 257, 377-
831 403. https://doi.org/10.1016/j.palaeo.2007.09.016
832
833 Westerhold, T., Röhl, U., McCarren, H. K., & Zachos, J. C. (2009). Latest on the absolute age of the
834 Paleocene - Eocene Thermal Maximum (PETM): New insights from exact stratigraphic position of
835 key ash layers +19 and -17. *Earth and Planetary Science Letters*, 287, 412-419.
836 https://doi.org/10.1016/j.epsl.2009.08.027
837
838 Westerhold, T., Röhl, U., Frederichs, T., Agnini, C., Raffi, I., Zachos, J. C., & Wilkens, R. H. (2017).
839 Astronomical calibration of the Ypresian timescale: implications for seafloor spreading rates and the
840 chaotic behavior of the solar system? *Climate of the Past*, 13, 1129-1152. https://doi.org/ 10.5194/cp-
841 2017-15
842
843 Yamaguchi, T., & Norris, R. D. (2012). Deep-sea ostracode turnovers through the Paleocene-Eocene
844 thermal maximum in DSDP Site 401, Bay of Biscay, North Atlantic. *Marine Micropaleontology*, 86-
845 87, 32-44. https://doi.org/10.1016/j.marmicro.2012.02.003
846

Zachos, J. C., Wara, M. W., Bohaty, S., Delaney, M. L., Petrizzo, M. R., Brill, A., et al. (2003). A transient rise in tropical sea surface temperature during the Paleocene-Eocene thermal maximum. *Science* 302, 1551-1554. https://doi.org/10.1126/science.1090110

Zachos, J. C., Röhl, U., Schellenberg, S. A., Sluijs, A., Hodell, D. A., Kelly, D. C., et al. (2005). Rapid acidification of the ocean during the Paleocene-Eocene thermal maximum. *Science*, 308, 1611-1615. https://doi.org/10.1126/science.1109004

Zeebe, R. E., Zachos, J. C., & Dickens, G. R. (2009). Carbon dioxide forcing alone insufficient to explain Palaeocene-Eocene Thermal Maximum warming. *Nature Geoscience*, 2, 576-580. https://doi.org/10.1038/NGEO578

Zeebe, R. E., Ridgwell, A., & Zachos, J. C. (2016). Anthropogenic carbon release rate unprecedented during the past 66 million years. *Nature Geoscience*, 9, 325-329. https://doi.org/ 10.1038/NGEO2681

Zhou, X., Thomas, E., Winguth, A. M. E., Ridgwell, A., Scher, H., Hoogakker, B. A. A., et al. (2016). Expanded oxygen minimum zones during the late Paleocene early Eocene: Hints from multiproxy comparison and ocean modeling. *Paleoceanography*, 31, 1532-1546. https://doi.org/10.1002/2016PA003020

FIGURES

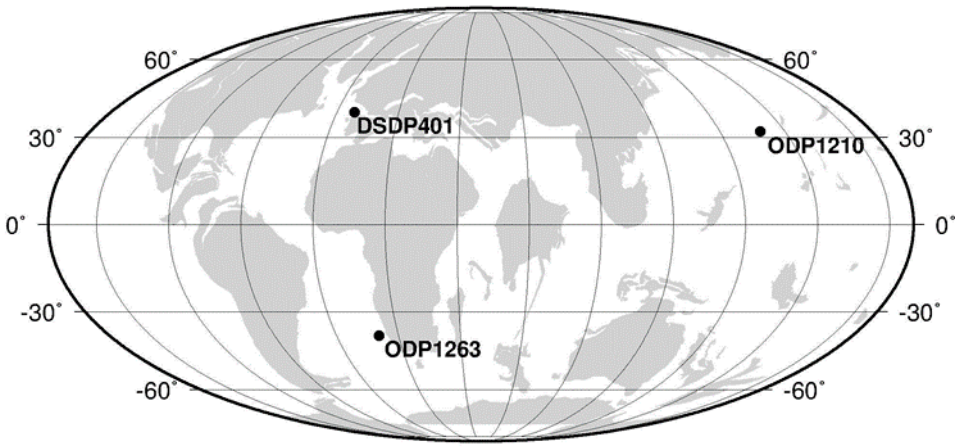

Figure 1: Palaeogeographic reconstruction for 56 Ma (www.odsn.de) with sample sites marked.

897

898

899

900

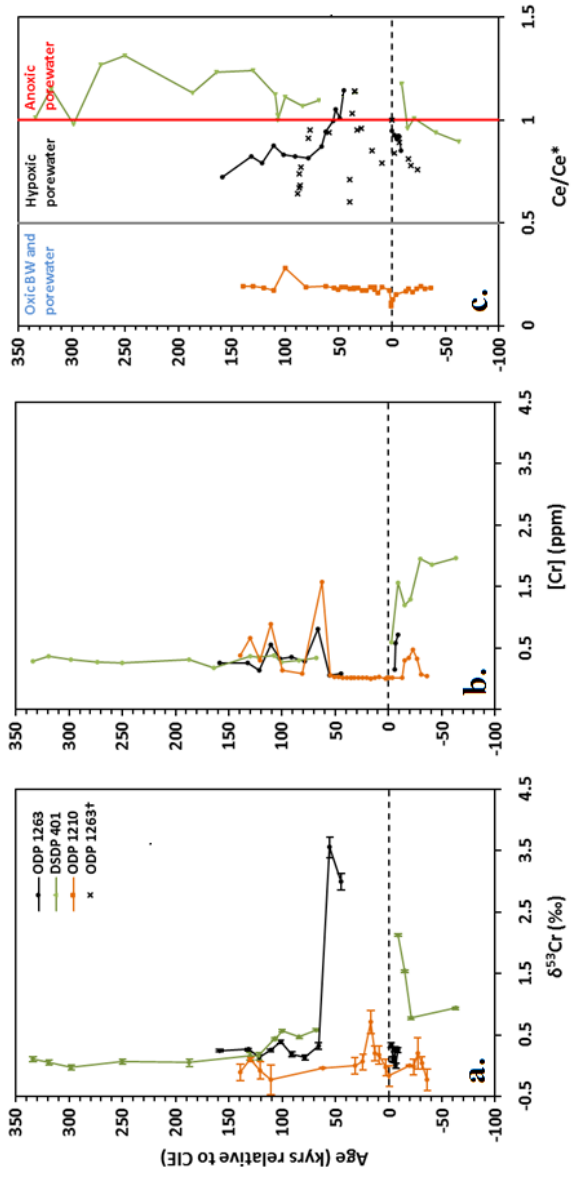

Figure 2: Records for Sites 401, 1210 and 1263 across the PETM of **a.** $\delta^{53}Cr$ (‰) show large differences in timing and size between the $\delta^{53}Cr$ excursions **b.** chromium concentrations (ppm) **c.** Cerium anomalies show that Northwest Pacific bottom waters were oxic and Atlantic bottom waters were hypoxic. Ce/Ce* above 1 indicates anoxic conditions and below 0.5 bottom waters are oxic (Haley et al., 2004). †Fish tooth Ce/Ce* data for ODP 1263 by Zhou et al. (2016). The dotted line corresponds to the onset of the CIE associated with the PETM. Tabled geochemical data can be found in supporting information A.

Figure 3: Records for Sites 401, 1210 and 1263 across the PETM of **a.** benthic $\delta^{13}C$ (‰) for Sites 401 and 1210 (Nunes and Norris, 2006; Westerhold et al., 2011), bulk $\delta^{13}C$ (‰) for Site 1263 (Zachos et al., 2005) **b.** benthic $\delta^{18}O$ (‰) from *N. truempyi* (Nunes and Norris, 2006; McCarren et al., 2008; Westerhold et al., 2011) **c.** Coarse fraction (> 63 μm) at Site 1263; a measure of $CaCO_3$ dissolution, measured for this study and in agreement with high resolution records by Kelly et al. (2010). The dotted line corresponds to the onset of the CIE associated with the PETM.

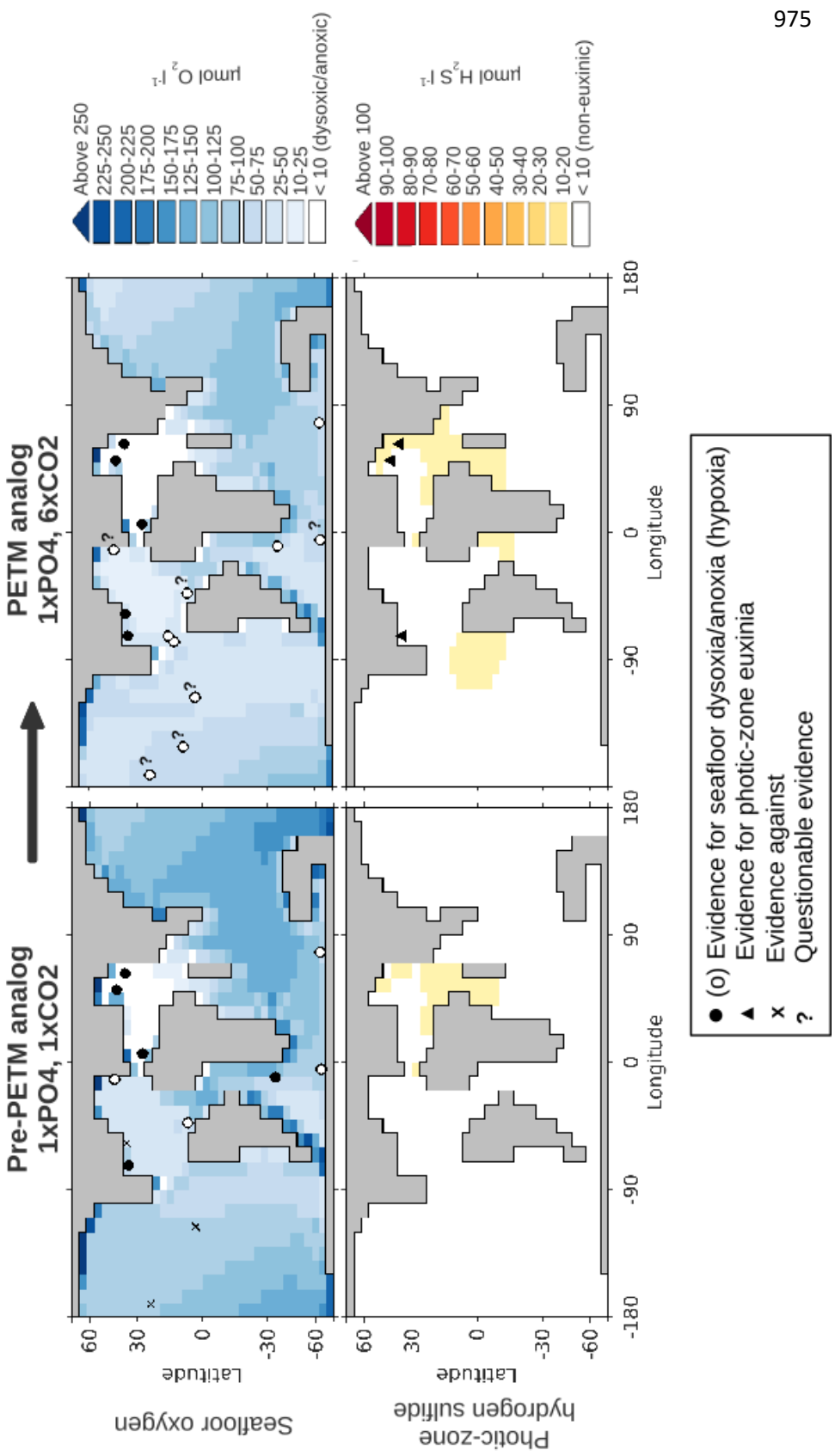

Figure 4: cGENIE model result for the best fit conditions for both before and during the PETM plotted with evidence for oxic seafloor environments (cross), seafloor hypoxia (open circle), seafloor anoxia (filled circle), and photic-zone euxinia (triangle). Non-conclusive sets of evidence have been marked by a question mark. The best model-data fits were achieved under 1x pre-industrial CO_2 values (1x CO_2) and 6x pre-industrial CO_2 values (6x CO_2) in the model. References for data points can be found in Carmichael et al., (2017) and includes Cr and Ce data from this study in addition. Model results indicate that up to 31% of the global ocean volume may have experienced hypoxic to anoxic conditions and suggest widespread open ocean deoxygenation took place during the PETM, whereas photic zone euxinia would have been restricted to the Eastern Tethys Sea and eastern boundary upwelling zones.

Oxygenation state	Ocean volume (%)	
	Pre-PETM	PETM
Anoxia/dysoxia	2	4
Hypoxia	12	27
Euxinia	4	8

Table 1 Summary of the findings of the cGENIE model-data comparison from this study on the percentage change in the global ocean's oxygenation state associated with the PETM.

Location	Method	Pre-PETM	PETM	Post PETM
DSDP Site 401 Bay of Biscay (North Atlantic)	**Ce/Ce***	Hypoxic	Anoxic	Anoxic
	δ^{53}Cr	Oxic	Hypoxic Anoxic	Oxic?
	cGENIE	Oxic	Hypoxic	-
	$^{\dagger}Mn_{EF}$ and U_{EF}	Suboxic	Suboxic	Suboxic
ODP Site 1210 Shatsky Rise (Pacific)	**Ce/Ce***	Oxic	Oxic	Oxic
	δ^{53}Cr	Oxic	Oxic	Oxic
	cGENIE	Oxic	Oxic	-
	$^{\dagger}Mn_{EF}$ and U_{EF}	Oxic	Oxic	Oxic
ODP Site 1263 Walvis Ridge (South Atlantic)	**Ce/Ce***	Hypoxic	Anoxic	Hypoxic
	δ^{53}Cr	Oxic	Hypoxic Anoxic	Oxic
	cGENIE	Oxic	Hypoxic	-
	$^{\dagger}Mn_{EF}$ and U_{EF}	Suboxic	Suboxic	Suboxic

Table 2 Summary of findings for the palaeo-redox state of the bottom waters at intermediate water depths during the PETM at DSDP Site 401, ODP Sites 1210 and 1263. Interpretations of the redox state are based on Ce/Ce* and δ^{53}Cr results from this study, cGENIE model-data comparison results from this study. $^{\dagger}Mn_{EF}$ and U_{EF} results are from Pälike et al. (2014). As the cGENIE model is spun-up towards a steady state, there is no 'post'-PETM assessment possible.

Figure 1.

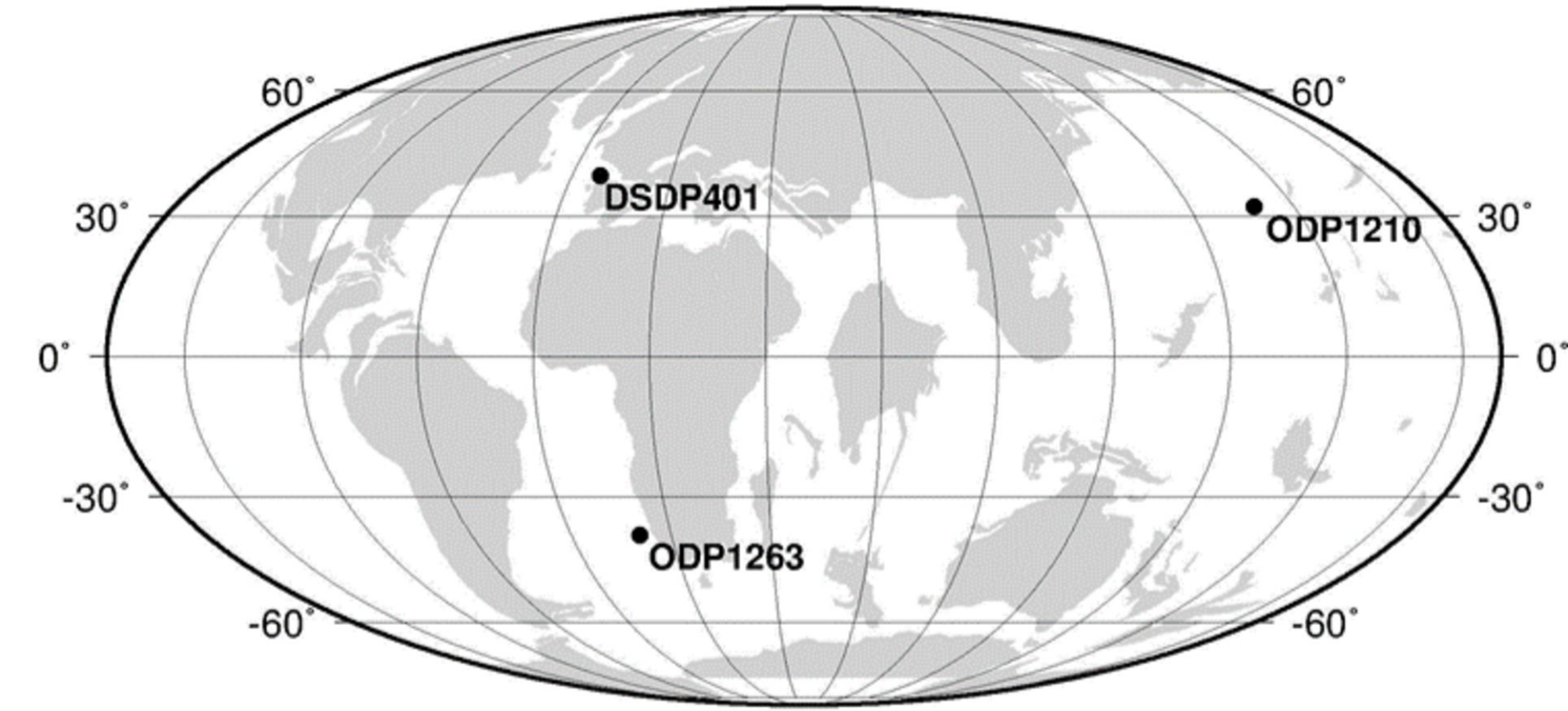
60˚
60˚
30˚
30˚
0˚
0˚
-30˚
-30˚
-60˚
-60˚
DSDP401
ODP1210
ODP1263

Figure 2.

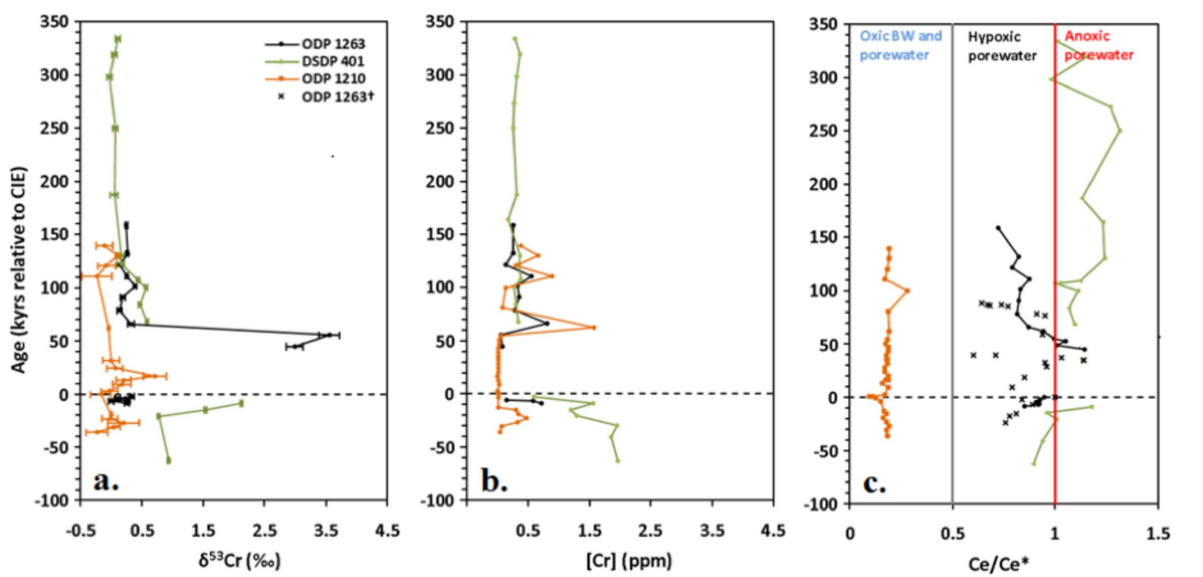
ODP 1263
DSDP 401
ODP 1210
ODP 1263†
Age (kyrs relative to CIE)
a.
δ53Cr (‰)
b.
[Cr] (ppm)
c.
Oxic BW and porewater
Hypoxic porewater
Anoxic porewater
Ce/Ce*

Figure 3.

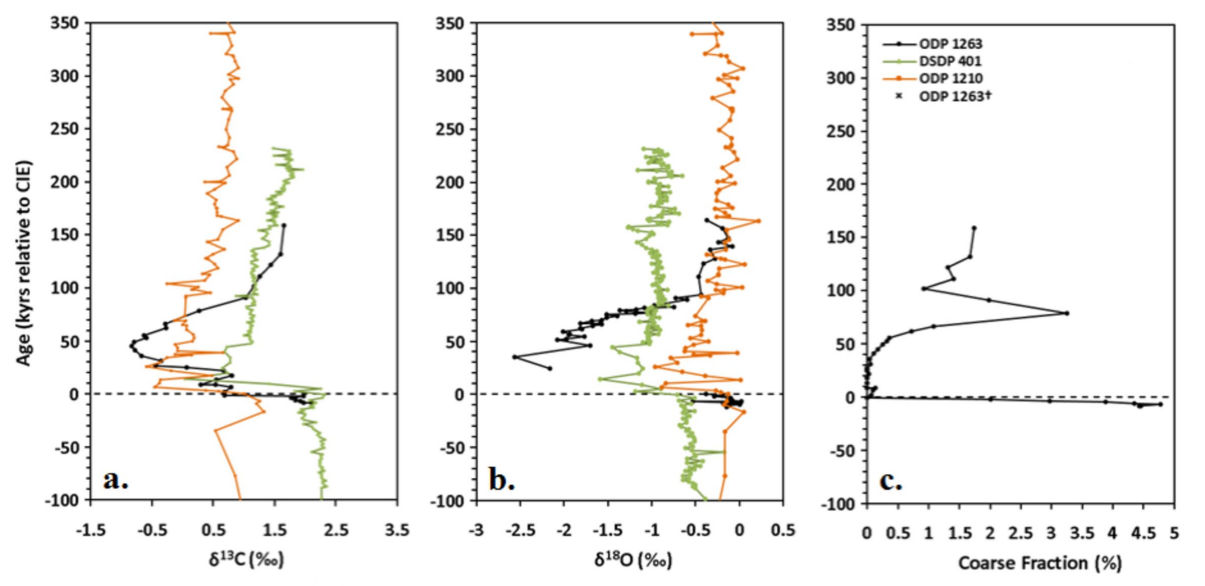
Age (kyrs relative to CIE)
350
300
250
200
150
100
50
0
-50
-100
a.
-1.5
-0.5
0.5
1.5
2.5
3.5
δ13C (‰)
b.
-3
-2.5
-2
-1.5
-1
-0.5
0
0.5
δ18O (‰)
ODP 1263
DSDP 401
ODP 1210
ODP 1263†
c.
0
0.5
1
1.5
2
2.5
3
3.5
4
4.5
5
Coarse Fraction (%)

Figure 4.

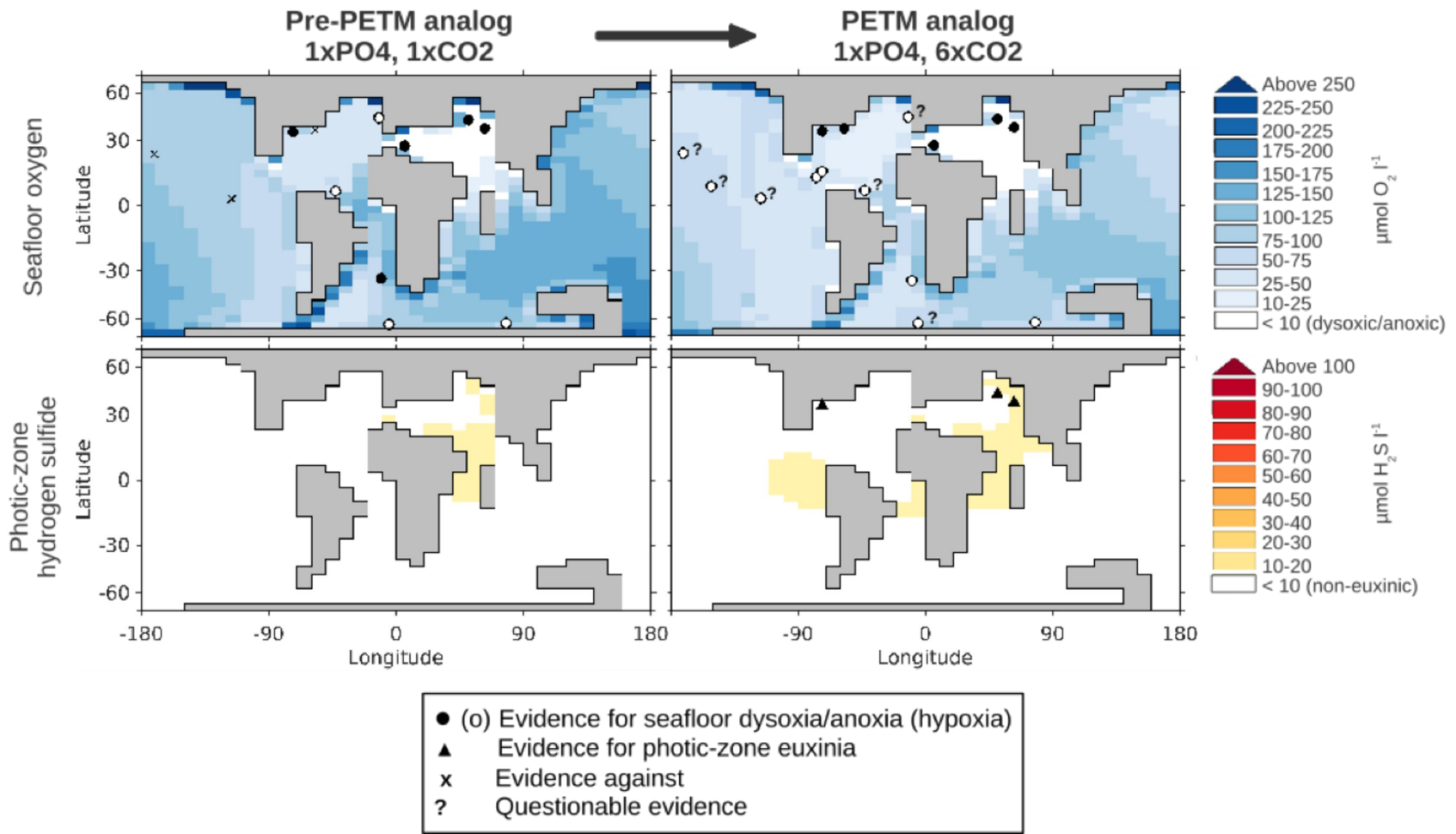
Pre-PETM analog
1xPO4, 1xCO2
PETM analog
1xPO4, 6xCO2
Seafloor oxygen
Photic-zone hydrogen sulfide
Latitude
Longitude
60
30
0
-30
-60
-180
-90
0
90
180
Above 250
225-250
200-225
175-200
150-175
125-150
100-125
75-100
50-75
25-50
10-25
< 10 (dysoxic/anoxic)
µmol O2 l-1
Above 100
90-100
80-90
70-80
60-70
50-60
40-50
30-40
20-30
10-20
< 10 (non-euxinic)
µmol H2S l-1
(o) Evidence for seafloor dysoxia/anoxia (hypoxia)
Evidence for photic-zone euxinia
Evidence against
Questionable evidence

Oxygenation state	Ocean volume (%)	
	Pre-PETM	PETM
Anoxia/dysoxia	2	4
Hypoxia	12	27
Euxinia	4	8

Location	Method	Pre-PETM	PETM	Post PETM
DSDP Site 401 Bay of Biscay (North Atlantic)	**Ce/Ce***	Hypoxic	Anoxic	Anoxic
	δ^{53}Cr	Oxic	Hypoxic Anoxic	Oxic?
	cGENIE	Oxic	Hypoxic	-
	$^{\dagger}Mn_{EF}$ and U_{EF}	Suboxic	Suboxic	Suboxic
ODP Site 1210 Shatsky Rise (Pacific)	**Ce/Ce***	Oxic	Oxic	Oxic
	δ^{53}Cr	Oxic	Oxic	Oxic
	cGENIE	Oxic	Oxic	-
	$^{\dagger}Mn_{EF}$ and U_{EF}	Oxic	Oxic	Oxic
ODP Site 1263 Walvis Ridge (South Atlantic)	**Ce/Ce***	Hypoxic	Anoxic	Hypoxic
	δ^{53}Cr	Oxic	Hypoxic Anoxic	Oxic
	cGENIE	Oxic	Hypoxic	-
	$^{\dagger}Mn_{EF}$ and U_{EF}	Suboxic	Suboxic	Suboxic